Advances in Science and Technology Research Journal, 2026, 20(1), 183–192 https://doi.org/10.12913/22998624/210707 ISSN 2299-8624, License CC-BY 4.0 Received: 2025.08.06 Accepted: 2025.09.14 Published: 2025.11.21

Spark plasma sintered titanium aluminum zirconium alloy for biomedical implant applications

Ekhlas Khalid Zamel¹, Hadar Al-Ethari¹, Ali Hubi Haleem^{1*}

- ¹ Metallurgical Engineering Department, College of Materials Engineering, University of Babylon, Iraq
- * Corresponding author's e-mail: akhlaskhalid93@gmail.com

ABSTRACT

Titanium-based alloys are among the most promising materials for biomedical applications due to their excellent mechanical properties, corrosion resistance, and biocompatibility. In this study, a Ti-2wt%Al-2.5wt%Zr alloy was synthesized using spark plasma sintering (SPS), a technique that enables rapid densification, precise microstructural control, and reduced porosity. The sintering was conducted at 950 °C with a heating rate of 100 °C/min under a pressure of 30 MPa, resulting in a fine and homogeneous microstructure with approximately 30% porosity, favorable for bone ingrowth and osseointegration. Microstructural analysis revealed the coexistence of α (HCP) and β (BCC) phases, providing an optimal combination of hardness and ductility. The alloy exhibited a Young's modulus of ~40 GPa, comparable to human cortical bone, minimizing the risk of stress shielding. Additionally, the surface hardness (~400 HV) and low corrosion rate (0.05 mm/year) indicated strong mechanical integrity and electrochemical stability. Although in-vitro cytotoxicity tests were not performed, the observed microstructure and corrosion behavior suggest promising biocompatibility. These results highlight the potential of the Ti–Al–Zr alloy produced via SPS for long-term orthopedic and dental implant applications.

Keywords: spark plasma sintering, Ti-Al-Zr alloy, biomedical implants, Young's modulus, osseointegration, orthopedic applications.

INTRODUCTION

Titanium (Ti) alloys have become one of the most preferred materials in biomedical applications due to their exceptional combination of properties, including high specific strength, low density, and outstanding corrosion resistance in physiological environments [1, 2]. Their ability to withstand long-term exposure to bodily fluids without degradation makes them highly biocompatible, enabling their use in orthopedic, dental, and surgical applications. Alloying titanium with elements such as aluminum (Al) and zirconium (Zr) further enhances these properties: Al increases structural strength without significantly adding weight, while Zr improves corrosion resistance and thermal stability [3]. These characteristics make Ti-Al-Zr alloys suitable for manufacturing load-bearing implants such as artificial joints, bone fixation plates, dental implants, and precision surgical tools [4–6].

Conventional fabrication techniques for Tibased alloys, such as traditional sintering, hot isostatic pressing (HIP), and localized heating sintering, are often limited by long processing times, high equipment costs, or microstructural inhomogeneity [7–9]. In contrast, Spark Plasma Sintering (SPS) offers rapid densification, precise control over microstructural evolution, and reduced defect formation, resulting in superior mechanical and physical properties [10–12].

Despite these advantages, the research on optimizing low-Al and low-Zr,Ti-Al-Zr alloys for biomedical applications remains limited. Systematic comparisons of the mechanical, corrosion, thermal, and biocompatibility performance of SPS-processed alloys against conventionally sintered counterparts are scarce in the literature.

Therefore, this study focused on the synthesis and characterization of Ti-2wt%Al-2.5wt%Zr alloy via SPS, evaluating its strength,

hardness, corrosion resistance, microstructure, density, thermal conductivity, and potential biocompatibility. By providing a detailed comparison with conventional sintering methods, this work aimed to bridge the current knowledge gap and demonstrate the capability of SPS as an efficient method for producing high-performance Ti-based biomaterials suitable for next-generation medical implants.

EXPERIMENT

Used materials and sample preparation

High-purity powders of titanium (Ti), aluminum (Al), and zirconium (Zr) with purities of 99.7%, 99.99%, and 99.9%, respectively, were used in this study. EDS results prove the purity of the powder, as shown in Figure 1.

XRD patterns show all characteristic peaks of the elements without extra peaks, which confirm the purity of the powders (Figure 2).

Particle size analysis was carried out for the powder via a laser particle size analyzer Type (Better size 2000) at the University of Babylon / College of Materials Eng. / Ceramics and Building Materials Labs. The analyses recorded 50,20 of 10 μm and for Ti, Al, and Zr, respectively.

The Ti-Al-Zr alloys were fabricated using the powder metallurgy (P/M) technique followed by spark plasma sintering (SPS). The Ti, Al, and Zr powders were blended using a planetary ball mill (Model: STGQM-15-2) at a speed of 300 rpm for 15 h under an argon atmosphere to prevent oxidation. Zirconium oxide (ZrO₂) balls with a hardness of 1400 MPa were employed as the milling media, with a

ball-to-powder weight ratio of 10:1. To avoid excessive temperature rise and powder agglomeration, the milling process was interrupted every 30 min for 10 min. A total milling duration of 15 h was selected based on preliminary trials and previous reports on the Ti-based alloys. Milling times shorter than 10 h resulted in insufficient homogeneity and incomplete particle refinement, whereas longer milling (>20 h) led to undesirable agglomeration and possible contamination from the milling media. Therefore, 15 h was considered an optimal compromise to achieve homogeneous mixing, enhanced mechanical activation, and refined particle size distribution without introducing significant contamination [13]. Localized heating and cold welding were followed by reverse rotation to ensure further homogenization. After milling, the powders were compacted via an electro-hydraulic press (Model: CT340-CT440, USA) in a 10 mm diameter steel die, applying a constant compaction pressure of 30 MPa. Two types of cylindrical green compacts were prepared: one with a diameter of 10 mm and a height of 3 mm for porosity, hardness, and microstructural analyses, and the other with a diameter of 10 mm and a height of 16 mm for compressive strength testing. The sintering process was carried out under a continuous flow of high-purity argon gas to prevent oxidation and preserve the microstructural integrity of the samples. The SPS sintering was performed at a temperature of 950 °C, with a heating rate of 100 °C/min and a duration of 5 minutes under a pressure of 30 MPa [14]. Figure3 illustrates the SPS sintering process and the compacted samples are illustrated in Figure 4.

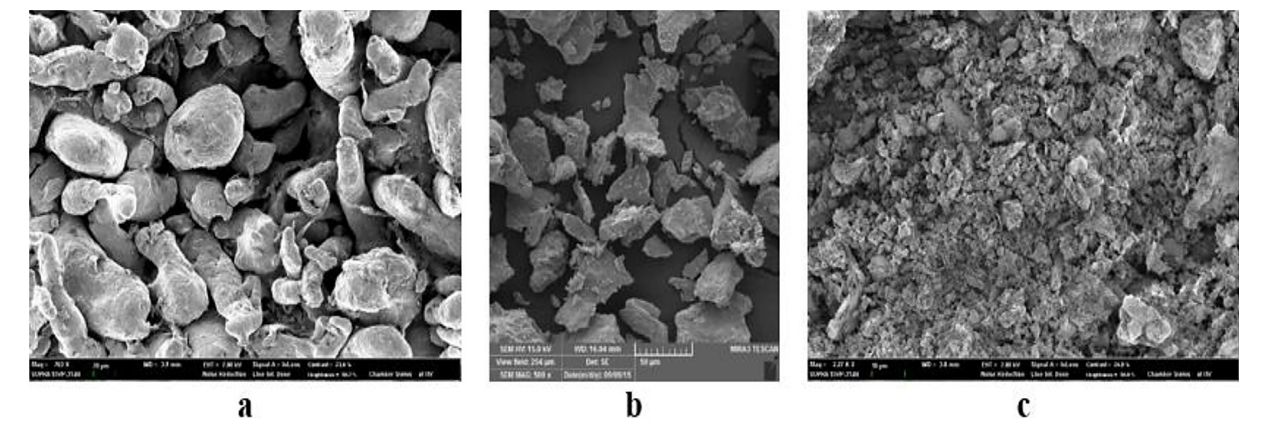


Figure 1. SEM images of the precursors: a-Al powder, b-Ti powder, and c-Zr powder

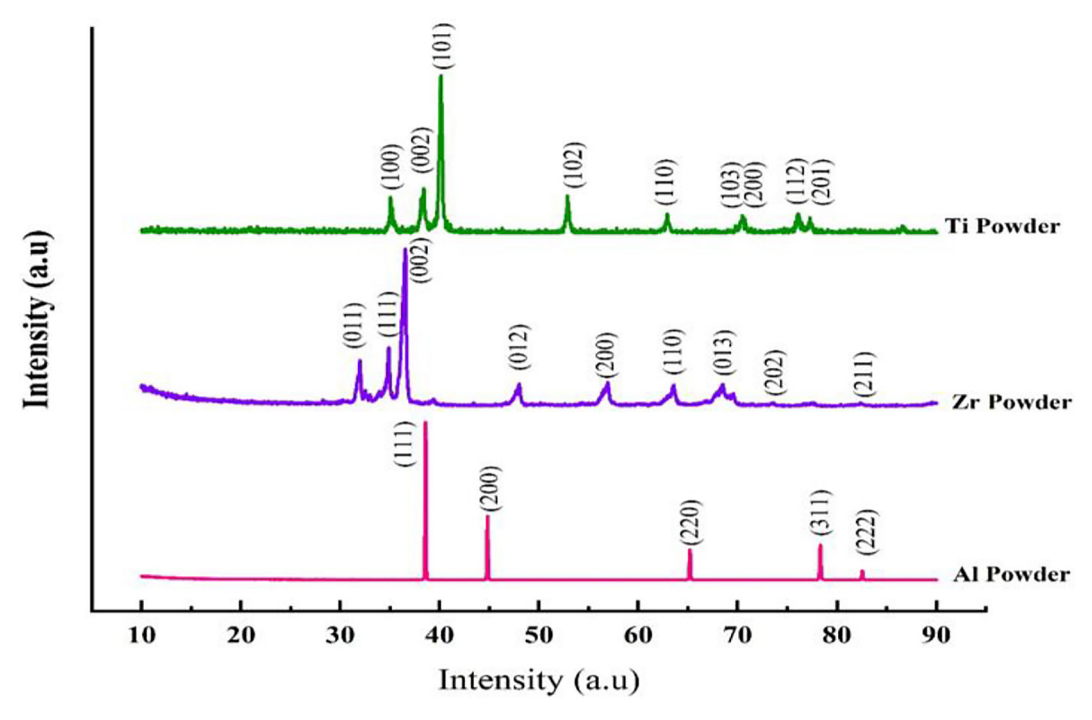


Figure 2. XRD Patterns of precursors

MECHANICAL AND PHYSICAL TESTS

Compression test

For the compression tests, specimens measuring 10 mm in diameter and 16 mm in length were created. According to ASTM (D695–85), the tests were conducted at room temperature using a general testing machine (WDW 200, No. W1124) with a loading speed of 0.5 mm/min, a compact pressure of 30 MPa, a sintering duration of 5 minutes, and an Al-Zr content of 2 and 2.5 percent.

Hardness test

ASTM E384 was followed for conducting the hardness test. To achieve a uniformly smooth surface, the specimens were polished after being sanded using the appropriate sanding papers. Using a diamond pyramid indenter at a 136° angle and a 62.5 N load, Vickers hardness was calculated as the average of three measurements.

True density and porosity after sintering

In accordance with ASTM (B328-96), the density specimen was dried for four hours at 120 °C and 10⁻⁴ Torr of pressure in a vacuum furnace. The weight of the dry sample was recorded as mass A once it had cooled to room temperature. The specimen was kept at room temperature

and immersed in oil (density Do = 0.8 g/cm³) for 30 minutes using a suitable evacuation pump. Weighing the fully impregnated specimen in air revealed that its mass was B. A specimen (mass, F) that has been completely impregnated with water was weighed.

Once the temperature has been recorded, the density of the water was determined. The investigation was carried out at a temperature of 30 °C, and at this temperature, the density of water (D_w) was 0.9956 g/cm³. Equation 1, 2 is used to calculate the density (D) [15].

$$D^{\circ} = \left(\frac{A}{B - F}\right) Dw \tag{1}$$

where: *D* is density, *A* mass of sintered sample, *B* mass of saturated sample and F mass of sample in water. The porosity (p) was calculated using Equation 2 [15].

$$P = \left(\frac{B - A}{(B - F)^{\circ} D} \times 100\right) Dw \tag{2}$$

Optical microscope (OM)

With the use of graded SiC papers (220, 320, 600, 800, 1000, 1200, 1500, 2000, 2500, and 3000), the specimens were wet ground. To achieve a smooth surface, they were subsequently

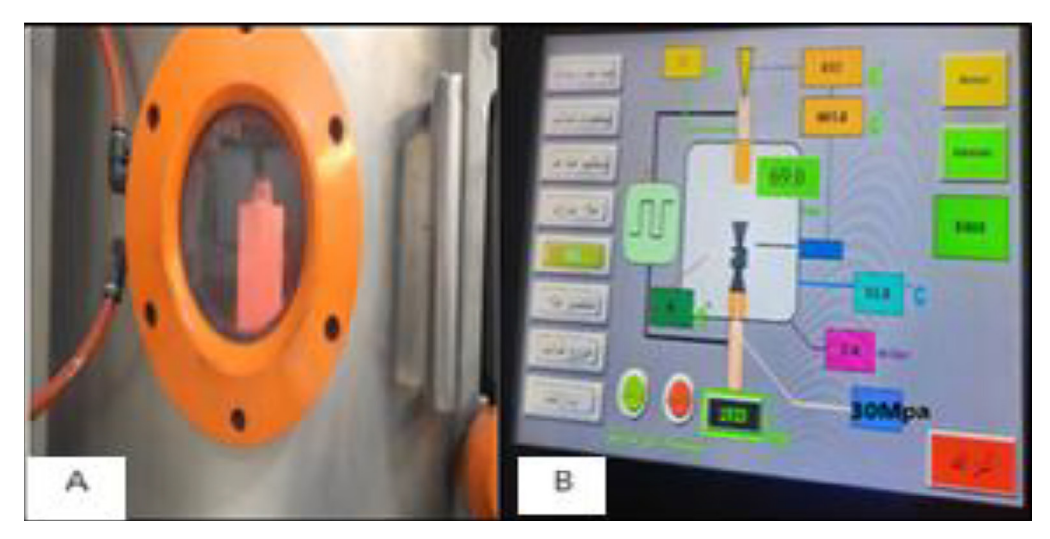


Figure 3. Sintering profile for SPS during work: A) the device viewing window showing the die containing the sample during heating in the SPS process; B) the digital control panel displaying temperature, pressure, current, and operating modes during SPS

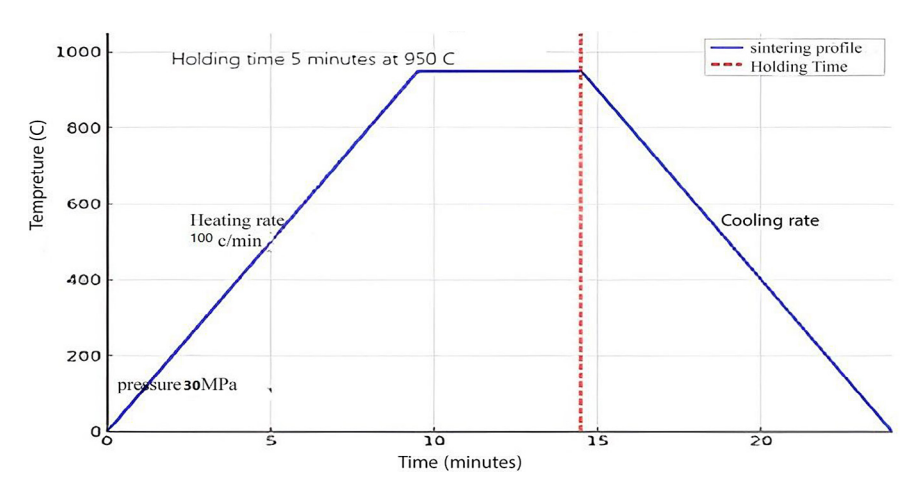


Figure 4. Sintering procedure of the compacted sample

polished with a diamond. The solution (3 ml HF + 6 ml HNO₃ + 100 ml H₂O) was used to etch the specimens at room temperature [16, 17]. The samples were cleaned and dried using distilled water and an electric dryer.

X-ray diffraction

In this study, the base alloy and the reinforced samples were characterized using X-ray diffraction (XRD 6000, Shimadzu, Japan). The measurements were carried out at an operating voltage of 40 kV and a current of 30 mA using Cu Kα radiation ($\lambda = 1.5405 \text{ Å}$). The scan was performed over a 2θ range of $20-80^{\circ}$, with a scanning rate of $6-7^{\circ}$ /min and a step size of 0.02° . The purpose of this analysis was to identify the phases formed in the sintered specimens.

The ultrasonic wave test

ASTM STP states that 696 [18] ultrasonic wave tests were performed to gauge the elastic characteristics of the sintered specimens. During the test, both high-wavelength and low-frequency pulses were used. Applying the values of the longitudinal and transverse velocities based on Equation 3 through 3 yielded elastic properties [19]:

$$v = [1-2(v_{T}/v_{T})^{2}]/[2-2(v_{T}/v_{T})^{2}]$$
 (3)

$$V_{L} = L/t \times 10^{-6} \tag{4}$$

$$E = \left[v_{L}^{2} \rho (1 + v) (1 - 2 v) \right] / (1 - v)$$
 (5)

where: V_T stands for transverse velocity (m/s), V_L for longitudinal velocity (m/s), and v for Poisson's ratio. L – specimen's length

(cm), and T – the time required to transfer longitudinal pulse through the specimen (s), E – modulus of elasticity (GPa), ρ – Density (kg/m³).

Linear polarization test

To investigate the corrosion of the prepared specimen in the human body, a corrosion test was carried out at 37 °C. The human bodily fluid was artificial Ringer's solution. At 37 °C, the pH value was 7.4. The test was carried out in compliance with ASTM G31-72 [20]. To achieve a smooth and scratch-free surface, a specimen measuring 10 mm in diameter and 3 mm in height was sanded and polished. The specimen was submerged in the solution during the test. For up to 40 minutes, the specimen's open circuit potential was measured. For the duration of the test, the voltage was recorded every five minutes.

Three-electrode cells with electrolytes of synthetic Ringer solution were used for electrochemical testing. Platinum served as the counter electrode, SCE as the reference electrode, and ASTM F746-04 [20] as the working electrode specimen. A plot was made of the potentiodynamic polarization curve. Tafel plots based on anodic and cathodic branches were used to determine the corrosion potential ($E_{\rm corr}$.) and corrosion current density ($I_{\rm corr}$.). To begin the test, a scanning rate of 0.2 mV/s was used for ± 250 mV at the open circuit potential (OCP) and above. The exam lasted for fourteen minutes. The corrosion rate was determined using Equation 6:

Corrosion rate (mpy) = $0.13I_{corr}(EW)/A.\rho$ (6) where: 0.13 – factor of conversion; Icorr. – corrosion current density (μ A/cm²); EW – equivalent weight (g); A – area (cm²); ρ – density (g/cm³); and mpy – corrosion rate (mils per year).

RESULTS AND DISCUSSION

Hardness tests

The high hardness value measured (400 HV) for the Ti-2Al-2.5Zr alloys used in biomedical applications can be attributed to several factors related to the preparation process using SPS and the intrinsic properties of the alloy itself. This result can be explained as follows – high densification

- SPS produces materials with densities close to theoretical values due to localized rapid heating and the applied sintering pressure, significantly reducing porosity. Grain refinement – the rapid sintering process reduces grain size, improving hardness according to the Hall-Petch relationship, where smaller grains enhance resistance to plastic deformation [21]. Homogeneous element distribution – SPS ensures a uniform distribution of added elements (e.g., Al and Zr), improving the material properties. The effects of added elements are as follows: (Al) – increases hardness by forming intermetallic compounds such as TiAl and Ti₃Al, which are characterized by their high hardness; zirconium (Zr) improves the thermal and mechanical stability of the alloy, enhancing deformation resistance and hardness properties. Matrix and added elements integration - the addition of Zr and Al can improve the interaction between phases, increasing the resistance of the material to mechanical deformation [21]. The obtained hardness value is comparable to or slightly higher than values reported for other SPS-processed biomedical titanium alloys. For instance, Walunj et al. [3] reported hardness values in the range of 360–390 HV for lightweight low-modulus Ti alloys produced via SPS, attributing the results to grain refinement and reduced porosity. Similarly, Zhu et al. [17] observed that the Ti-25Nb-6Zr alloys fabricated at optimal SPS temperatures exhibited hardness values of approximately 380 HV, emphasizing the role of Zr in enhancing mechanical stability. In addition, Gao et al. [4] demonstrated that precise control of powder morphology and densification during processing can lead to superior mechanical performance in Ti alloys, a trend consistent with the high hardness obtained in the present study. These comparisons confirm that the current Ti-2Al-2.5Zr composition achieves competitive hardness levels, likely due to its balanced α/β phase ratio and uniform microstructure.

High hardness values are critical for improving wear resistance in biological environments. Enhanced hardness reduces wear caused by friction or chemical interactions, making the alloy more suitable for medical applications such as bone and dental implants. Previous reviews, such as Annur et al. [22], have highlighted that hardness above $\sim\!350$ HV significantly increases the longevity of the load-bearing implants. In the present study, the higher proportion of the α phase increases hardness, while an appropriate amount of the β phase enhances toughness [23].

Porosity and density

The sintering process resulted in an apparent density of 3.161 g/cm³, which is significantly lower than the theoretical density of the alloy (4.516 g/cm³). This noticeable discrepancy indicates the presence of internal voids, likely caused by incomplete consolidation of powder particles during the sintering stage. Such porosity is a common and expected feature in the materials fabricated using powder metallurgy techniques [8, 12].

In certain biomedical applications, this controlled porosity contributes to the transport of physiological fluids and supports biological integration at the implant site, thereby enhancing the functional performance of the implant within the biological environment [24].

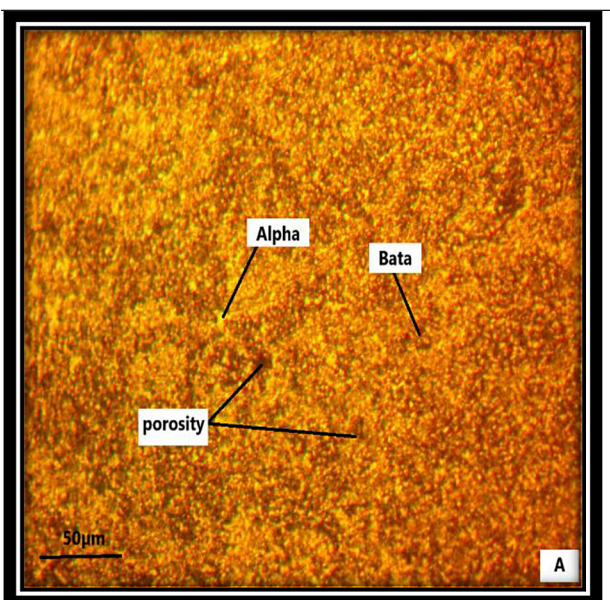
The calculated difference in density corresponds to a final porosity level of approximately 30%, which falls within the acceptable and even favorable range for biomedical applications, such as dental and orthopedic implants. This level of porosity facilitates fluid transport and enables bone tissue ingrowth within the porous structure, thereby promoting osseointegration and contributing to long-term biological fixation [25]. Similar findings were reported by Annur et al. [26], who highlighted that controlled porosity between 25-35% in SPS-processed titanium alloys enhances bone in growth without significantly compromising mechanical integrity. Furthermore, Zhu et al. [19] observed that Ti-Nb-Zr alloys with 28-32% porosity exhibited excellent biocompatibility and adequate strength for load-bearing applications, supporting the suitability of the porosity range achieved in the present work. Despite the presence of this porosity, the alloy retains sufficient mechanical strength to withstand physiological loads, with minimal compromise in toughness or hardness. This balance between the mechanical performance and biological functionality enhances the suitability of the Ti-Al-Zr alloy for medical implant applications. Previous research by Gao et al. [4] demonstrated that optimizing powder consolidation and pore distribution during fabrication can further improve both mechanical reliability and biological response, in agreement with the current findings. Therefore, the observed porosity plays a critical role in supporting both the structural integrity and biocompatibility of the material, making it a promising candidate for clinical use in load-bearing biomedical implants [25].

The optical microstructure

The optical microstructure of the sintered samples compacted at 30 MPa is shown in Figure 5. The microstructure is predominantly composed of the α-titanium phase, which provides excellent corrosion resistance and biological stability. Dark regions correspond to retained β-phase and residual porosity after sintering. A fine-grained structure resulting from the short sintering duration (5 min). Such porosity, when maintained within an optimal range (~30%), facilitates osseointegration by allowing the transport of biological fluids and enhancing the adhesion and proliferation of bone cells on the alloy surface [27]. However, excessive porosity may compromise fatigue resistance, which should be carefully considered in the design of long-term implants. Aluminum acts as an α-phase stabilizer, improving corrosion resistance and biodegradation stability, while zirconium contributes to enhanced biocompatibility. These combined effects make the SPS-produced alloy promising for biomedical applications, such as bone and joint implants, offering a favorable balance of strength, biocompatibility, and long-term durability [29-31]. Furthermore, the refined grain structure is consistent with previous reports, indicating that controlling the sintering time in SPS reduces grain growth and improves both mechanical and biological properties [29, 32].

X-Ray diffraction results

The XRD pattern illustrates the phase analysis of the Ti-Al-Zr alloy sintered by Spark Plasma Sintering (SPS), identifying the various crystalline phases present based on the positions and angles of the diffraction peaks. The primary α phase (α-Ti), which possesses a hexagonal closepacked (HCP) structure, is clearly detected. Additionally, the β phase (β -Ti) with a body-centered cubic (BCC) structure is observed. The β phase typically forms at high temperatures or in the presence of alloying elements, such as Zr, which stabilizes this phase even at lower temperatures [30]. Sharp peaks in the XRD pattern indicate the presence of large grains or a well-ordered crystalline structure, whereas broad peaks suggest small grains or a nanostructured material, a characteristic commonly observed in the materials fabricated using techniques such as SPS [31]. SPS significantly promotes the formation of stable and homogeneous phases due to its rapid heating



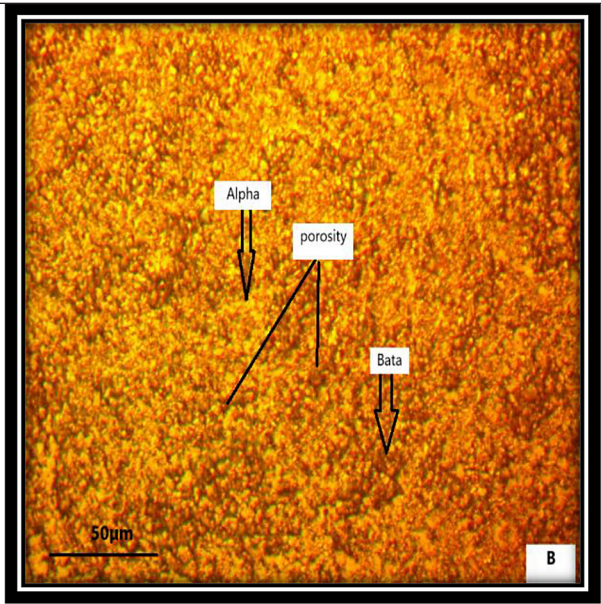


Figure 5. Magnified optical micrographs of the Ti-2Al-2.5Zr alloy sintered at 30 MPa A) 200 x; B) 400x

rates and applied high pressure, which enhances the mechanical properties of the alloy. These attributes make Ti-Al-Zr alloys particularly suitable for medical applications, offering a balanced combination of high strength and excellent corrosion resistance [32, 33]. This synergy of properties ensures that Ti-Al-Zr alloys provide both durability and biocompatibility, making them ideal candidates for biomedical implants (Figure 6).

Results of ultrasonic wave test

The Ti–2Al–2.5Zr alloy produced via SPS exhibited a reduced elastic modulus (E = 40 GPa) close to that of human cortical bone (~30 GPa), compared to pure titanium (~105 GPa), which helps minimize stress shielding. This reduction is largely attributed to the relatively high porosity (~30%) of the alloy, induced by SPS, which lowers stiffness while enhancing osseointegration potential. Although below the typical range reported for titanium alloys (60–120 GPa), these results indicate promising suitability for biomedical implants, with further mechanical testing on fully dense samples recommended to confirm reliability [34, 35].

Open circuit potential (OCP)

The potential fluctuation of the alloy sample in Ringer's solution over time is shown in Figure 7. The alloy reached a steady-state potential after approximately 35 min, which can be attributed to the formation of a protective oxide layer on the surface. The initial fluctuations in potential suggest the nucleation and growth of this passive film. Once stabilized, the alloy maintained a relatively stable open-circuit potential, which indicates its ability to resist corrosion in a simulated physiological medium.

Although the short exposure time (35 min) provides only preliminary insight into corrosion behavior, these results are consistent with the previously reported studies on Ti-based biomedical alloys [36]. To strengthen the interpretation, further long-term immersion or electrochemical impedance spectroscopy (EIS) analyses are recommended. Nevertheless, the observed behavior supports the suitability of the fabricated alloys as potential candidates for biomedical implants.

Test of linear polarization

The Ti-Al-Zr alloy prepared by SPS demonstrates excellent corrosion resistance, as confirmed by the potentiodynamic polarization test in Ringer's solution shown in Figure 8.

The measured corrosion potential (E_{corr}) of -321~mV indicates stable electrochemical behavior, while the extremely low corrosion current density (I_{corr}) of 20.68 nA/cm² corresponds to a very slow corrosion rate of 0.05 mpy result shown in Table 1.

This outstanding performance can be attributed to the formation of a protective oxide film, further stabilized by the presence of zirconium and aluminum, as well as to the microstructural refinement induced by SPS processing.

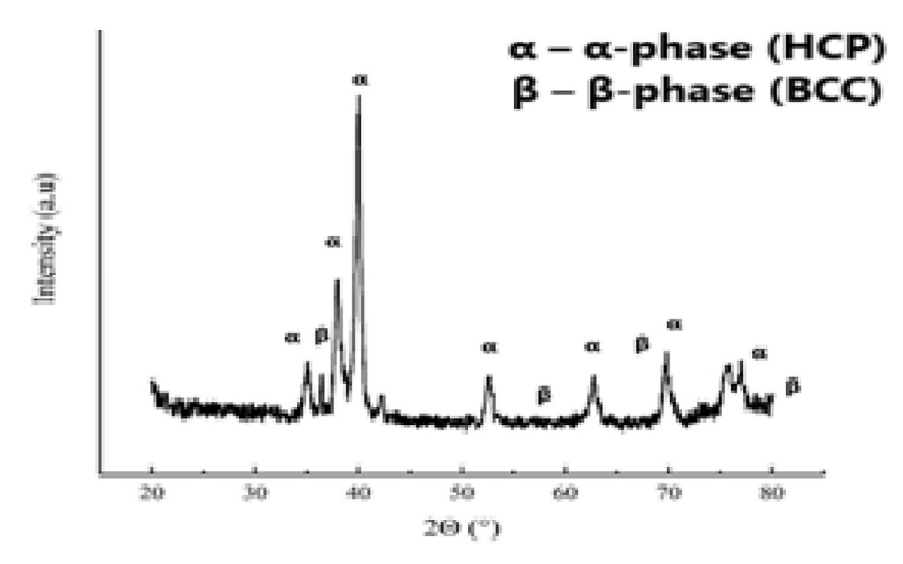


Figure 6. XRD pattern of the sintered Ti-Al-Zr alloy

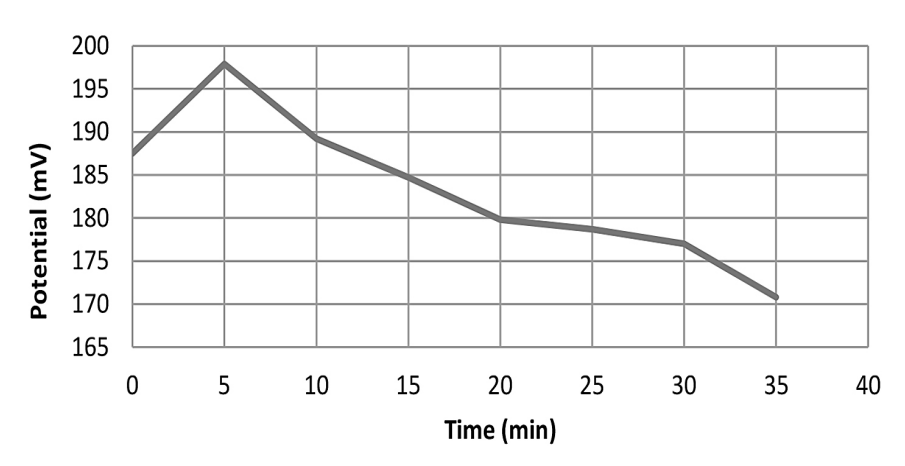


Figure 7. Corrosion potential of the Ti-2Al-2.5Zr alloy fabricated by SPS, measured in Ringer's solution for 30 minutes

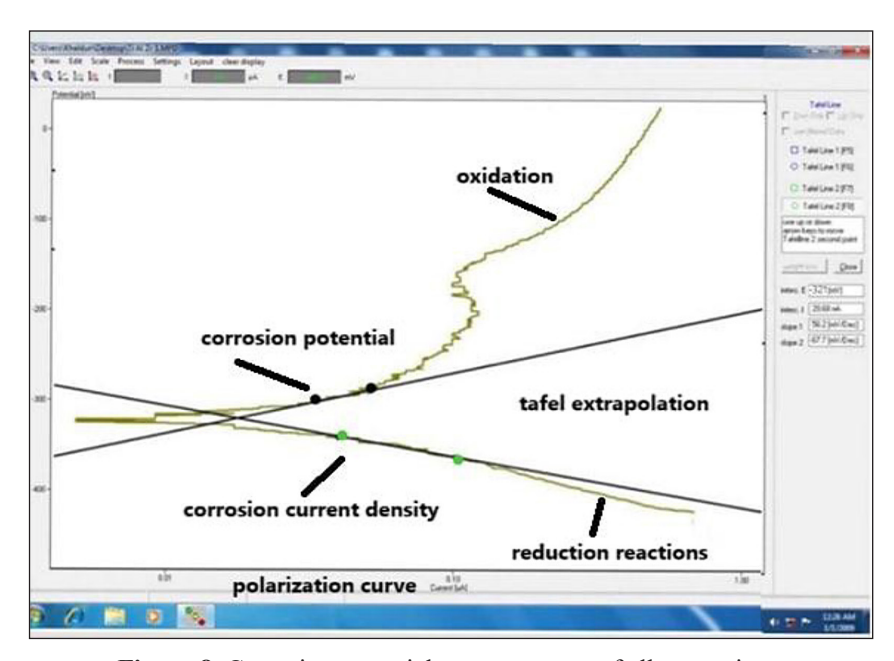


Figure 8. Corrosion potential measurements of alloy specimen

700 1 1 4	a .		C .1			'.1 CD' C A 1 43 7
Table 1.	Corrosion	narameters (of the s	necimen	comparision	with Ti6Al4V

Sample	Ecorr [mv]	Icorr [μΑ\cm²]	Corrosion rate (mpy)
Ti-Al-Zr	-321	20.68	0.05
Ti-6Al4V	-322	200	

When compared with the conventional Ti-6Al-4V alloy, the superiority of Ti-Al-Zr becomes evident. The reported data show that Ti-6Al-4V exhibits significantly higher Icorr values, ranging between 200 and 2000 nA/cm² depending on the heat treatment conditions, with corrosion rates around 0.01 mpy or higher in Ringer's solution [1–3]. These results clearly demonstrate that the Ti-Al-Zr alloy not only exhibits more stable passivation behavior but also provides enhanced protection in simulated physiological environments, making it a promising candidate for biomedical implant applications [37].

CONCLUSIONS

The Ti-2Al-2.5Zr alloy fabricated by SPS showed:

- Enhanced mechanical performance with higher strength and lower elastic modulus, closer to that of natural bone, reducing stress shielding risks.
- 2. Excellent corrosion resistance due to the formation of a stable oxide layer in simulated body fluids.
- 3. Improved biocompatibility, making it a strong candidate for orthopedic, dental, and surgical implants.
- 4. Demonstrated advantages of SPS as an efficient technique for producing low Al–Zr titanium alloys with superior properties compared to conventional sintering.

REFERENCES

- Marin E, Lanzutti A. Biomedical applications of titanium alloys: a comprehensive review. Materials. 2023;17:114. https://doi.org/10.3390/ma17010114
- Zhang J, Guo W, Zhang Y, Guo Q, Wang C, Zhang L. Mechanical properties and phase structure of (TiAlZr)N films deposited by multi arc ion plating. Thin Solid Films. 2009;517:4830–4834. https://doi. org/10.1016/j.tsf.2009.04.044
- 3. Walunj G, Desai J, Bohara S, Contieri R, Kothapalli C, Ivanov E, Borkar T. Light weight-low

- modulus biocompatible titanium alloys processed via spark plasma sintering. J Alloys Metallurg Syst. 2023;3:100018. https://doi.org/10.1016/j.jallcom.2023.170018
- Gao S, Korzhyk V, Strohonov D, Tereshchenko O, Demianov O, Ganushchak O. Evaluation of the possibility of obtaining spherical powders of titanium alloy Ti 6Al 4V by supersonic reverse polarity plasma torch for use in additive manufacturing. Adv Sci Technol Res J. 2025;19:434–448. https://doi.org/10.12913/22998624/205855
- Bandopadhyay S, Bandyopadhyay N, Ahmed S, Yadav V, Tekade RK. Current research perspectives of orthopedic implant materials. In: Biomaterials and Bionanotechnology. Elsevier; 2019;337–374.
- 6. Tapscott DC, Wottowa C. Orthopedic implant materials. 2020.
- Liu YZ, Zu XT, Li C, Qiu SY, Huang XQ, Wang LM. Surface characteristics and corrosion behavior of Ti–Al–Zr alloy implanted with Al and Nb. Corros Sci. 2007;49:1069–1080. https://doi.org/10.1016/j. corsci.2006.08.008
- Danninger H, Calderon RDO, Gierl-Mayer C. Powder metallurgy and sintered materials. Addit Manuf. 2017;19:12–22. https://doi.org/10.1016/j. addma.2017.03.001
- Bocanegra-Bernal MH. Hot isostatic pressing (HIP) technology and its applications to metals and ceramics. J Mater Sci. 2004;39:6399–6420. https://doi. org/10.1023/B:JMSC.0000043343.17917.a1
- Cavaliere P, Sadeghi B, Shabani A. Spark plasma sintering: process fundamentals. In: Spark plasma sintering of materials: advances in processing and applications. 2019;3–20.
- Ratzker B, Sokol M. Exploring the capabilities of high-pressure spark plasma sintering (HPSPS): a review of materials processing and properties. Mater Des. 2023;233:112238. https://doi.org/10.1016/j. matdes.2023.112238
- 12. Tokita M. Spark plasma sintering (SPS) method, systems, and applications. In: Handbook of advanced ceramics. 2013;1149–1177.
- 13. Fouzia H, Mamoun F, Naouel H, Linda A, Goussem M, Said M, et al. The effect of milling time on the microstructure and mechanical properties of Ti-6Al-4Fe alloys. Mater Today Commun. 2021;27:102428. https://doi.org/10.1016/j.mtcomm.2021.102428
- 14. Liang SJ, et al. Microstructure evolution and mechanical properties of Ti-6Al-4Zr-4Nb alloys

- by spark plasma sintering. Metall Mater Trans A. 2024;55(7):3125–3137. https://doi.org/10.1007/s11661-024-07879-9
- 15. ASTM B328-96. Standard test method for density, oil content, and interconnected porosity of sintered metal structural parts and oil-impregnated bearings. West Conshohocken (PA): ASTM International; 1996.
- Al-Ethari H, Abbas S, Zamel EK. Optimization of manufacturing titanium—magnesium alloy for biomaterial applications using grey relational analyses. IOP Conf Ser Mater Sci Eng. 2021;1094:012148. https://doi.org/10.1088/1757-899X/1094/1/012148
- Zhu Q, Chen P, Xiao Q, Li F, Yi J, Prashanth KG, Eckert J. Mechanical properties and microstructural evolution of Ti-25Nb-6Zr alloy fabricated by spark plasma sintering at different temperatures. Metals (Basel). 2022;12:1824. https://doi.org/10.3390/met12111824
- Jafari J, Zebarjad SM, Sajjadi SA. Effect of prestrain on microstructure of Ni–Ti orthodontic archwires. Mater Sci Eng A. 2008;473:42–48. https:// doi.org/10.1016/j.msea.2007.03.019
- 19. Bidhendi HRA, Pouranvari M. Corrosion study of metallic biomaterials in simulated body fluid. Metall Mater Eng. 2012;31:13–22. https://doi.org/10.63278/mme.v31.1
- 20. Hiromoto S. Corrosion of metallic biomaterials. In: Metals for biomedical devices. Woodhead Publishing; 2019;131–152.
- 21. Musi M, Kardos S, Hatzenbichler L, Holec D, Stark A, Allen M, et al. The effect of zirconium on the Ti-(42–46 at.%) Al system. Acta Mater. 2022;241:118414. https://doi.org/10.1016/j.actamat.2022.118414
- 22. Annur D, Kartika I, Supriadi S, Suharno B. Titanium and titanium based alloy prepared by spark plasma sintering method for biomedical implant applications a review. Mater Res Express. 2021;8:012001. https://doi.org/10.1088/2053-1591/abcf8c
- 23. Upadhyaya GS. Powder metallurgy technology. Cambridge: Cambridge International Science Publishing; 1997.
- 24. Rechtin J, Torresani E, Ivanov E, Olevsky E. Fabrication of titanium—niobium—zirconium—tantalium alloy (TNZT) bioimplant components with controllable porosity by spark plasma sintering. Materials (Basel). 2018;11:181. https://doi.org/10.3390/ma11020181
- 25. Slokar Benić L, Komljenović L, Erman Ž, Jajčinović M. Analysis of the densification of a biomedical titanium alloy produced by powder metallurgy. In: IX International Scientific Congress Innovations 2023; 2023 Jun; [place unknown]. Scientific-Technical Union of Mechanical Engineering; 2023. p. 113–116.
- 26. Williams ML. CRC Handbook of Chemistry and

- Physics. 76th ed. Occup Environ Med. 1996;53:504. https://doi.org/10.1136/oem.53.7.504
- 27. Hulbert DM, Anders A, Andersson J, Lavernia EJ, Mukherjee AK. A discussion on the absence of plasma in spark plasma sintering. Scr Mater. 2009;60:835–838. https://doi.org/10.1016/j.scriptamat.2009.01.02
- 28. García-Hernández C, García-Cabezón C, González-Diez F, Ampudia M, Juanes-Gusano D, Rodriguez-Cabello JC, Martín-Pedrosa F. Effect of processing on microstructure, mechanical properties, corrosion and biocompatibility of additive manufacturing Ti-6Al-4V orthopaedic implants. Sci Rep. 2025;15:14087. https://doi.org/10.1038/s41598-025-14087
- 29. Munir ZA, Anselmi-Tamburini U, Ohyanagi M. The effect of electric field and pressure on the synthesis and consolidation of materials: a review of the spark plasma sintering method. J Mater Sci. 2006;41:763– 777. https://doi.org/10.1007/s10853-006-6553-1
- 30. Welsch G, Boyer R, Collings EW, editors. Materials properties handbook: titanium alloys. Materials Park (OH): ASM International; 1993.
- 31. Niinomi M. Biologically and mechanically biocompatible titanium alloys. Mater Trans. 2008;49:2170–2178. https://doi.org/10.2320/matertrans.M2008083
- 32. Cullity BD, Stock SR. Elements of X-Ray Diffraction. New York: Prentice-Hall Inc.; 2001.
- Orrù R, Licheri R, Locci AM, Cincotti A, Cao G. Consolidation/synthesis of materials by electric current activated/assisted sintering. Mater Sci Eng R Rep. 2009;63:127–187. https://doi.org/10.1016/j.mser.2008.08.003
- 34. Taniguchi N, Fujibayashi S, Takemoto M, Sasaki K, Otsuki B, Nakamura T, et al. Effect of pore size on bone ingrowth into porous titanium implants fabricated by additive manufacturing: an in vivo experiment. Mater Sci Eng C. 2016;59:690–701. https://doi.org/10.1016/j.msec.2015.10.024
- 35. Hayyawi AR, Al-Ethari H, Haleem AH. Characterization of biomedical Ti-35Nb-5Ta-7Zr alloy prepared by powder metallurgy route. Can Metall Q. 2024; [Epub ahead of print]:1–12.
- 36. Nokhrin A, Andreev P, Boldin M, Chuvil'deev V, Chegurov M, Smetanina K, et al. Investigation of microstructure and corrosion resistance of Ti-Al-V titanium alloys obtained by spark plasma sintering. Metals (Basel). 2021;11:945. https://doi.org/10.3390/met1106094
- 37. Singh PK, Kumar S, Jain PK, Dixit US. Effect of heat treatment on electrochemical behavior of additively manufactured Ti-6Al-4V alloy in Ringer's solution. J Mater Eng Perform. 2024;33(18):9570–9582. https://doi.org/10.1007/s11665-024-0999